Int J Fract (2011) 167:57–70
DOI 10.1007/s10704-010-9519-0

ORIGINAL PAPER

Analysis and computations of oscillating crack propagation in a heated strip

Thomas Menouillard · Ted Belytschko

Received: 8 February 2010 / Accepted: 2 June 2010 / Published online: 26 June 2010

Abstract This paper presents a computational analysis and several simulations of an existing experiment, which deals with a quasi-static thermal crack propagation in a glass plate. The experimental observation was that a straight or oscillatory crack propagation occurred depending on the plate width and thermal loading. The goal here is to simulate this experiment with the recent numerical tool such as XFEM. First, the analysis of the settings of the experiment is developed by providing the computed energy release rate of the crack for a wide range of experiment settings parameters. Second, different crack propagations are simulated, and show a good agreement with the experimental observation of straight or oscillatory paths. Third, a study of the results given by the fracture criteria (maximum hoop stress and Local Symmetry criteria) is also presented for this particular experiment in order to evaluate their differences.

Keywords Temperature · Crack propagation · Quasi-static · Energy release rate · Oscillatory path · Instability

T. Menouillard (✉) · T. Belytschko
Northwestern University, Theoretical and Applied Mechanics, 2145 Sheridan Road, Evanston, IL 60208-3111, USA
e-mail: t-menouillard@northwestern.edu

T. Belytschko
e-mail: tedbelytschko@northwestern.edu

Nomenclature

$a, \dot{a}$	Crack length and velocity
t	Time
T	Temperature
$\underline{\underline{\sigma}}$	Stress tensor
$\underline{\underline{\varepsilon}}$	Strain tensor
$\underline{\underline{\mathbb{C}}}$	Linear elastic behavior law
$\underline{\underline{I_d}}$	Identity matrix
K_1, K_2	Stress intensity factors
θ_c	Crack angle
G	Energy release rate

Material properties

α	Coefficient of thermal expansion
ρ	Density
E	Young's modulus
ν	Poisson's ratio
k	Thermal conductivity
D	Thermal diffusivity
c_p	Specific heat capacity
c_r	Rayleigh wave speeds
K_{Ic}	Fracture toughness
G_c	Critical energy release rate

Experiment parameters

z	Vertical position of the crack tip
T_{hot}	Temperature of the oven
T_{cold}	Temperature of the water
$\Delta T = T_{hot} - T_{cold}$	Temperature difference
V	Dipping velocity

h Distance water-oven
w Plate width

1 Introduction

Thermally driven cracks have been the topic of many experimental studies, because it is a topic of both scientific and practical interest. Bahr et al. (1986) studied thermal shock cracking in ceramic where the fracture models were based on the concept of the energy release rate. Yuse and Sano (1993) showed by experiment that a crack can be driven by a thermal loading without any mechanical loading, and in addition an instability in the crack path can occur for specific geometries of the specimen. Marder (1994) set up an experiment to show this instability in the crack propagation. He dealt with a long precracked glass plate traveling from an oven into a water bath at ambient temperature. He observed that for a temperature gradient great enough, the crack propagates and the crack tip remains in the region between the cold water and the oven when the plate slowly moves from the oven to the water bath. He also studied the relation between the fracture energy and the dipping velocity. He showed a dependence with the dipping velocity and compared his values with the literature (Griffith 1921; Reddy et al. 1988). He also noticed that above 5 mm/s some 3D effects occurred in the glass, even as thin as 1 mm in the experiment, and the fracture energy became difficult to evaluate. Ronsin et al. (1995) presented an experimental study of thermal crack propagation and the description of their results in term of crack paths: straight or oscillatory paths depending on the plate width. They used a soda lime glass plate, and the dipping velocity was controlled by a stepping motor, paced by a TTL (transistor transistor logic) clock signal. The cold region consisted of a bath of 30 l of water at ambient temperature. Ronsin and Perrin (1997) studied simultaneous propagation of crack in glass under thermal loading, and more particularly the crack spacing depending on the plate width and number of cracks in the plate. Ronsin and Perrin (1998) studied a single crack and performed temperature measurements in situ in the glass plate for different dipping velocities to ensure a good agreement with crack model. They studied the propagation as a function of the plate width and the dipping velocity. Their observation was that an oscillating crack propagation occurred when the plate width was greater than a critical value; below that, the crack propagated straight if the temperature gradient was sufficient. More recently, Deegan et al. (2003) performed the same experiment to show the different kinds of propagation in the glass. In addition to the straight and oscillatory crack paths, they also observed a branching crack in such an experiment for a higher temperature gradient.

In parallel, to the experimental research, many theoretical studies have been made. Adda-Bedia and Pomeau (1995) presented the first theoretical approaches where a conservative linear elasticity calculation was introduced to deal with the straight to oscillatory transition. Sasa et al. (1994) presented a theory, and their results globally agreed with the experimental observations. Pla (1996) described the thermal crack propagation theory in a general point of view. Bahr et al. (1995) studied the transition between the straight and the oscillatory crack propagation. Also Yoneyama et al. (2008) studied the transition using an initial perturbation in the crack direction with the kink angle theory (Cotterell and Rice 1980). However the theoretical analysis of this experiment is still an active topic according to the recent literature (Pham et al. 2008; Corson et al. 2009).

In term of numerical simulations concerning this experiment, the literature is quite light. Ferney et al. (1999) presented a numerical simulation of oscillatory and branching crack growth in glass plates for this same experiment. They used the cohesive element method (Needleman 1987) and they showed oscillatory crack paths and even observed branching cracks. However their results presented a significant mesh dependence in the crack path. Recently, Kilic and Madenci (2009) presented numerical results using peridynamic theory.

In this paper, we present a computational analysis of the experiments and also simulate the different kinds of crack propagation, i.e. straight and oscillating. We use the extended finite element method (XFEM) (Belytschko and Black 1999; Moës et al. 1999), which provides the numerical tool which will allow to describe any path independently of the mesh of the structure.

The paper is organized as follows. Section 2 presents the experiment and observations according to the literature. Section 3 briefly presents the space discretization and the time integration for introducing the numerical tool. Section 4 describes an analysis of the experiment parameters such as the loading and the geometry, and relates them to the energy release rate which indicates

whether or not a crack propagation will occur. Section 5 presents the numerical simulation of crack propagations for this experiment, dealing with the different types: straight and oscillating. Section 6 presents the concluding remarks.

2 The experiment

2.1 Experiment setup

The experiment is described by a long glass specimen whose width w and thickness $e = 1.1$ mm moving at velocity V from an oven at temperature $T_{hot} \in [135; 200°C]$ which is typical of these experiments Marder (1994), to a cold water at ambient temperature $T_{cold} = 20°C$. The temperature difference ΔT between the oven and the water bath is defined by $\Delta T = T_{hot} - T_{cold}$. V is called the dipping velocity. The distance between the oven and the water bath is denoted by h. Fig. 1 shows the geometry of the experiment and the four parameters of the experiment: h, w, ΔT and V. Table 1 presents the material properties of the glass.

The geometry is defined by: $h \in [3; 10\text{ mm}]$, $w \in [3; 30\text{ mm}]$. The loading is defined by the temperature difference $\Delta T \in [0; 260°C]$ and the dipping velocity is $V \in [0.01; 10\text{ mm/s}]$. An experiment is defined by a set of four values $\{h,\ \Delta T,\ w,\ V\}$ remaining constant during the experiment.

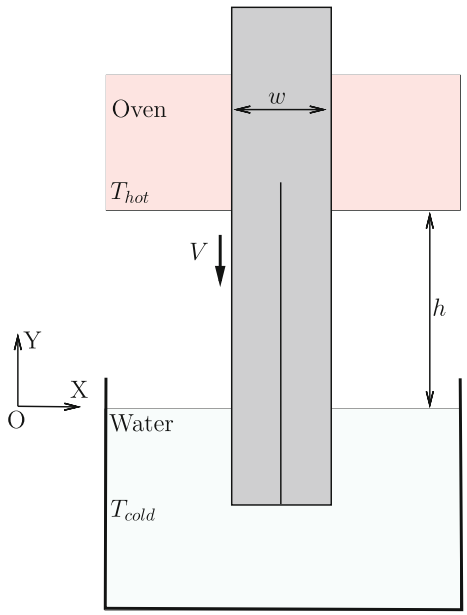

Fig. 1 Geometry and loading of the experiment

Table 1 Materials properties of glass

Material properties	Symbol	Value
Young's modulus	E	75 GPa
Poisson's ratio	ν	0.23
Density	ρ	2, 500 kg/m^3
Thermal expansion	α	$7.7.10^{-6}$ /K
Thermal diffusivity	D	$0.47.10^{-6}$ m$^2/s$
Specific heat capacity	c_p	870 J/K/kg
Thermal conductivity	k	1.022 J/m/s/K
Fracture toughness	K_{Ic}	0.33 MPa$\sqrt{\text{m}}$

2.2 Thermal analysis

We assume a linear elastic behavior of the glass and we do not consider any crack in the specimen in this section. The general thermal equation is:

$$\begin{cases} \dfrac{\partial T}{\partial t} + V\dfrac{\partial T}{\partial Y} + D\left(\dfrac{\partial^2 T}{\partial X^2} + \dfrac{\partial^2 T}{\partial Y^2} + \dfrac{\partial^2 T}{\partial Z^2}\right) = 0 \quad \text{in } \Omega \\ T = T_{hot} \quad \text{if } Y > h \\ T = T_{cold} \quad \text{if } Y < 0 \text{ and} \\ \quad \left(|Z| = \frac{e}{2} \text{ or } |X| = \frac{w}{2}\right) \end{cases} \tag{1}$$

where $D = \frac{k}{\rho c_p}$ denotes the thermal diffusivity of the glass, t the time, ρ the density, k the thermal conductivity, and c_p the specific heat capacity. Note that V is positive and opposite to the Y direction. X and Y are the coordinates in basis shown in Fig. 1. Note the coordinates (X, Y) are spatial coordinates attached to the laboratory but not to the glass plate. Thus there is no time dependence in the temperature field, because the thermal steady case is considered: $\frac{\partial T}{\partial t} = 0$ thus the temperature is written $T(X, Y, Z)$.

First we assume a one dimensional thermal problem. Thus the temperature depends on the vertical coordinates Y only, and Eq. (1) becomes:

$$V\frac{\partial T}{\partial Y} + D\frac{\partial^2 T}{\partial Y^2} = 0 \tag{2}$$

The boundary conditions allow to obtain:

$$T(Y) = \begin{cases} T_{cold} & \text{if } Y < 0 \\ T_{hot} + (T_{cold} - T_{hot}) & \\ \quad \dfrac{e^{-\frac{Y}{d}} - e^{-\frac{h}{d}}}{1 - e^{-\frac{h}{d}}} & \text{if } 0 < Y < h \\ T_{hot} & \text{if } h < Y \end{cases} \tag{3}$$

where $d = \frac{D}{V}$.

Second a 2D (i.e. (Y, Z) plane in Fig. 1) computational analysis of the temperature through the thickness of the glass plate (i.e. Z direction in Fig. 1) is performed. The associated variational formulation is given by the use of an arbitrary field denoted by T^*:

$$\int_\Omega \left(\frac{\partial T}{\partial t} T^* + V \frac{\partial T}{\partial Y} T^* - D \nabla T^* \cdot \nabla T \right) d\Omega = D \int_{\partial \Omega_2} T^* \Phi_2 dS \tag{4}$$

One obtains for a steady case and the boundary condition a single system to solve. Figure 2 shows the analytical result of Eq. (2) for a 1D thermal analysis; it also shows that for small velocity V (less than 0.1 mm/s) the temperature field is almost linear in the vertical direction Y. Figure 2 also shows the temperature computed with a 2D simulation. The result shown in Fig. 2 is the temperature at the center of the specimen at $Z = 0$. One can conclude that the 1D analytical and the 2D simulation give similar results for small dipping velocities. Moreover both 1D analytical and 2D numerical results agree well with the experiment measurement in situ performed by Ronsin and Perrin (1998). Nevertheless there is a slight difference near $Y = 0$ because of the difference between the 1D and 2D boundary conditions. However the tensile region created by the thermal stress is located near the entrance of the oven, i.e. near $y = 5$ mm in this particular case in Fig. 2. In this region, the 2D and 1D solutions are very similar. For the following study, only small dipping velocities (less than 0.1 mm/s) are considered. Therefore the temperature field in the glass between the water and the oven is linear (see Fig. 2).

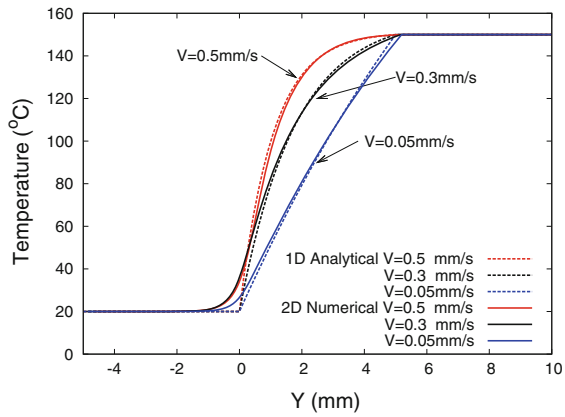

Fig. 2 Temperature as a function of the vertical position for different dipping velocity V: to be compared with Ronsin and Perrin (1998):$T_{hot} = 150°C$, $T_{cold} = 20°C$ and $h = 5$ mm

2.3 Experimental observations

The temperature field in the plate creates a tensile stress near the entrance of the oven (Ronsin and Perrin 1998). This is the reason why the crack may propagate when its tip is located in this region. As the dipping velocity is quite low (less than 0.1 mm/s compared to the Rayleigh wave speed), the crack may propagate quasi-statically at the same dipping velocity, but in the opposite direction. Thus, the crack tip remains in the region of the entrance of the oven.

The experimental observations were noted on the crack path patterns. Indeed a straight crack propagation is expected according to the boundary conditions and quasi-static loading. However a curious crack path was observed: by increasing the plate width or the thermal loading, the crack propagation leaves its straight behavior to turn into an oscillatory crack path (Ronsin et al. 1995; Ronsin and Perrin 1998). In addition, Yang and Ravi-Chandar (2001) and Deegan et al. (2003) also observed some crack branching for high temperature jumps.

3 Space discretization and time integration for numerical simulation

The simulation is performed with a regular 4-node element mesh: the element size is 0.5 mm. The temperature is imposed in the structure according to the previous section. We only consider very small dipping velocity, so that there is no dependence on the dipping velocity. The variation of the strain tensor denoted by $\underline{\underline{\varepsilon}}$ is due to the temperature field in the structure $\delta T = T - T_{hot}$. A linear isotropic elastic material law denoted by a fourth order tensor $\mathbb{C}$ is used to model the material behavior as following:

$$\underline{\underline{\sigma}} = \mathbb{C} : \left(\underline{\underline{\varepsilon}} - \alpha \, \delta T \, \underline{\underline{I_d}} \right) \tag{5}$$

where $\underline{\underline{\sigma}}$ denotes the stress tensor, and $\underline{\underline{I_d}}$ the identity matrix.

The extended finite element method (XFEM) (Belytschko and Black 1999; Moës et al. 1999; Belytschko et al. 2001) based on the finite element method, is used to model the crack in the space discretization.

The advantage is that no remeshing nor projection are required when the crack propagates through the mesh. Any mesh is expected to perform well with any straight or oscillatory crack path, because this method avoids mesh dependence.

Although the experiment is quasi-static, the time integration is based on the explicit central difference method (Belytschko et al. 2000). A lumped mass matrix is used to speed up the computation and avoid at inversing the mass matrix (Menouillard et al. 2006, 2008) at each time step. In order to compute until physical time 600 s in a reasonable time, an artificial density is used to perform faster the quasi-static simulation; the virtual density is taken to be one billion times the real one. The corresponding virtual dilatational wave speed becomes 173 mm/s which is still bigger by more than two orders than the dipping velocity V. Therefore the critical time step becomes 2 ms and the computation can be run in a reasonable time. Ferney et al. (1999) chose to use a dipping velocity of 1, 000 m/s instead. Their numerical time were also artificial. These two approaches perform the computation in the same number of steps. As we do not aim at studying the effect of the dipping velocity V, these computations remain physical.

4 Analysis of the experimental parameters in term of energy release rate

4.1 Energy release rate and crack law

Let consider the energy release rate G defined by the variation of the dissipated energy through the crack propagation per unit of surface. The relation between the energy release rate and the stress intensity factors denoted by K_1 and K_2, is given by:

$$G = \frac{1}{E'}\left(K_1^2 + K_2^2\right) \tag{6}$$

where $E' = E$ in plane stress, and $E' = E/(1-\nu^2)$ in plane strain. The stress intensity factors are determined via the J-integral (Rice 1968): this path independent integral J is numerically computed with a virtual extension vector whose direction β is the same than the crack. To determine both stress intensity factors, two equations are written, and they correspond to the projection of the displacement field $\mathbf{u}$ onto both mode 1 and 2 asymptotic displacement fields $\mathbf{u}_1$ and $\mathbf{u}_2$ (Attigui and Petit 1997; Menouillard et al. 2006) as:

$$K_p = \frac{E}{1-\nu^2} J_\beta(\mathbf{u}, \mathbf{u}_p) \qquad \forall p \in \{1, 2\} \tag{7}$$

The crack velocity law is given by Freund (1972):

$$\frac{\dot{a}}{c_r} = \begin{cases} 1 - \frac{G_c}{G} & \text{if } G > G_c \\ 0 & \text{otherwise.} \end{cases} \tag{8}$$

where c_r is the Rayleigh wave speed, and G_c denotes the critical energy release rate. In addition, the direction of the crack (see Erdogan and Sih 1963 for more discussion on the criterion) can be driven by the maximum hoop stress criterion or the Local Symmetry criterion (Gol'dstein and Salganik 1974) (sometimes named the "$K_2 = 0$ criterion"):

- The maximum hoop stress criterion is an explicit criterion because the crack direction θ_c is directly given by the stress intensity factors K_1 and K_2 as:

$$\theta_c = 2\arctan\left[\frac{1}{4}\left(\frac{K_1}{K_2} - sign(K_2)\sqrt{8 + \left(\frac{K_1}{K_2}\right)^2}\right)\right] \tag{9}$$

- The Local Symmetry criterion is based on the theory that the crack always propagates in the direction where the mode 2 stress intensity factor vanishes. This principle was originally described by Gol'dstein and Salganik (1974) and generalized under general assumptions by Adda-Bedia et al. (1999). This criterion was also derived by Hakim and Karma (2009) in the context of phase field models without assuming it a priori, and successfully used even for random cracks (Katzav et al. 2007). It is an implicit criterion because there is no direct formulation. The direction is obtained with a converging algorithm evaluating a direction ensuring that the mode 2 stress intensity factor K_2 is zero in the evaluated direction.

Algorithm 1 presents the determination of the new crack direction with both the Maximum hoop stress criterion and the Local Symmetry criterion criterion. This emphasizes the need of a loop to converge to the direction whose mode 2 stress intensity factor vanishes. This also shows that the relation between the maximum hoop stress criterion and the Local Symmetry criterion in this algorithm: the maximum hoop stress stress criterion is the result of the first loop, whereas the Local Symmetry criterion corresponds to the result after converging: typically five to seven loops give a converged solution.

Algorithm 1 Maximum hoop stress and Local Symmetry criteria.

$\theta_c^{(0)} = 0$
$\beta^{(0)} \leftarrow \beta$ {β is the direction of the crack}
$i \leftarrow 0$ {Initialization of the counter i}
repeat
  $\beta^{(i+1)} \leftarrow \beta^{(i)} + \theta_c^{(i)}$ {New direction of the virtual extension field in the J-integral}
  $K_1^{(i+1)} \leftarrow J_{\beta^{(i+1)}}(\mathbf{u}, \mathbf{u}_1)\, E/(1-\nu^2)$ {Mode 1 stress intensity factor, i.e. Eq. (7)}
  $K_2^{(i+1)} \leftarrow J_{\beta^{(i+1)}}(\mathbf{u}, \mathbf{u}_2)\, E/(1-\nu^2)$ {Mode 2 stress intensity factor, i.e. Eq. (7)}
  $\theta_c^{(i+1)} \leftarrow f(K_1^{(i+1)}, K_2^{(i+1)})$ {maximum hoop stress criterion, i.e. Eq. (9)}
  $i \leftarrow i + 1$
until $K_2^{(i+1)} = 0$ {Numerical use of a tolerance instead}
$n \leftarrow i$ {n is the number of iterations}
print "Maximum hoop stress criterion gives:"
print "Mode 1 and 2 stress intensity factors: " $K_1^{(1)}$ and $K_2^{(1)}$
print "Turning angle of the crack is " $\theta_c^{(1)}$
print "Local Symmetry criterion gives:"
print "Mode 1 stress intensity factor: " $K_1^{(n)}$ {and $K_2^{(n)} = 0$}
print "Turning angle of the crack is " $\theta_c^{(n)} = \sum_{i=1}^{n} \theta_c^{(i)}$

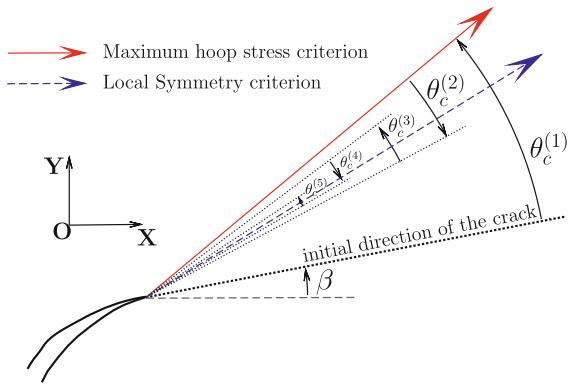

Fig. 3 Explanation of Algorithm 1 in term of crack direction determination

Figure 3 shows the description of the algorithm in term of turning angle near the crack tip for each iteration, and how the algorithm converges. It also presents the following numerical observation:

$$| \theta_c^{(n)} | \leq | \theta_c^{(1)} | \tag{10}$$

This means that the angle given by the Local Symmetry criterion is always smoother/smaller than the one given by the maximum hoop stress criterion.

Although the principles of symmetry and maximum hoop stress can give similar results for some experiments, they deviate for kinking cracks (Amestoy and Leblond 1992; Katzav et al. 2007). Section 5.2.2 presents a study of the numerical results given by both criteria for this particular experiment of a crack in a heated strip.

4.2 Energy release rate as a function of the distance water-crack tip

For a given plate width w and a temperature difference ΔT, the energy release is computed as a function of the distance water-crack tip denoted by z without allowing the crack to propagate. Figure 4 presents the energy release rate as a function of the distance water-crack tip for different gap water-oven h. It shows that the energy release rate is non zero near the entrance of the oven and always presents a maximum value, denoted by $G_{\max}$, at a distance a little smaller than h. This maximum indicates whether or not the crack will propagate.

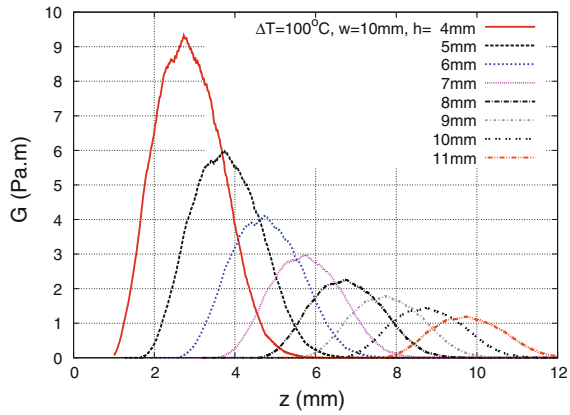

Fig. 4 Energy release rate as a function of the distance water-crack tip z for different h, with $T_{hot} = 120°\text{C}$, $T_{cold} = 20°\text{C}$ and $w = 10$ mm

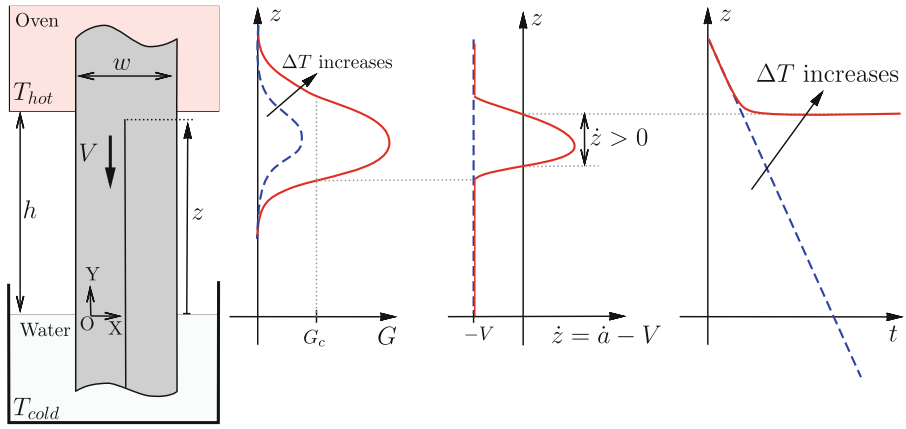

Fig. 5 Energy release rate and velocity of the vertical position of the crack tip as a function of the vertical position of the crack tip, and vertical position of the crack tip as a function of time

Indeed, if the maximum of the energy release rate is greater than the critical value G_c, a crack propagation should occur.

Figure 5 describes the stability of the vertical position of the crack tip controlled by the energy release rate which directly gives the crack velocity through Eq. (8) and by the dipping velocity. The vertical position of the crack tip is denoted by z and depends on the time t. Indeed the system is:

$$\begin{cases} \dot{z} = \dot{a} - V \\ z(0) = z_0 >> h \end{cases} \tag{11}$$

where $\dot{a}$ is the crack velocity, and V the dipping velocity of the glass in the $-Y$ direction. The initial condition $z(t = 0) >> h$ means that whole precracked specimen is initially in the oven. In addition the precrack length has to be at least the distance water-oven h.

Let us now study the dependence of the maximum of the energy release rate denoted by $G_{\max}$ with the experimental parameters h, ΔT and w. The dependence with the dipping velocity is not studied in the paper. Only very small dipping velocities are considered (i.e. 0.1 mm/s).

4.3 Maximum of the energy release rate as a function of the temperature and distance water-oven

Multiple simulations, such as the ones shown in Fig. 4, have been run to establish some dependences between the maximum of the energy release rate and the parameters of the experiment. Figure 6 presents the maximum of the energy release rate as a function of the distance water-oven h and the temperature difference ΔT for four different plate widths: (a) $w = 12$ mm, (b) $w = 10$ mm, (c) $w = 8$ mm and (d) $w = 6$ mm.

The results presented in Fig. 6 are reported in Fig. 7 in a different manner. Figure 7 shows the maximum of the energy release rate as a function of the ratio $(\Delta T/h)^2$. Figure 7 clearly points out a linear dependence of the maximum of the energy release rate with the temperature gradient $(\Delta T/h)$ square.

Beside this, the dependence with the Young's modulus and the coefficient of thermal expansion are quite easy to determine; the relation between the energy release rate and the Young's modulus is linear as linear elastic material model is considered, and the relation with the coefficient of thermal expansion α is the same than the temperature ΔT, because they always appear together (see Eq. 5). One can conclude that: a function f, whose unit is m^3, depending on w, exists so that

$$G_{\max} = E \left(\frac{\alpha \Delta T}{h} \right)^2 f(w) \tag{12}$$

4.4 Maximum of the energy release rate as a function of the plate width

According to Buckingham's pi-theorem Buckingham (1915), a relation exists between the previous variables and $G_{\max}$ based on the analysis of the unit system as:

$$G_{\max} \# E \left(\alpha \Delta T \frac{w}{h} \right)^2 w \tag{13}$$

Figure 8a presents the ratio corresponding to Eq. (13). It shows that for a quite significant range of $h \in [3; 11$ mm$]$ and $\Delta T \in [60; 160°\text{C}]$ the ratio is only represented by a dot in Fig. 8a for a specific plate width. For example, the dot shown at $w = 10$ mm and $ratio = 0.0033$ is actually composed of 88 dots: each combination of $h \in \{4, 5, 6, 7, 8, 9, 10, 11$ mm$\}$ and

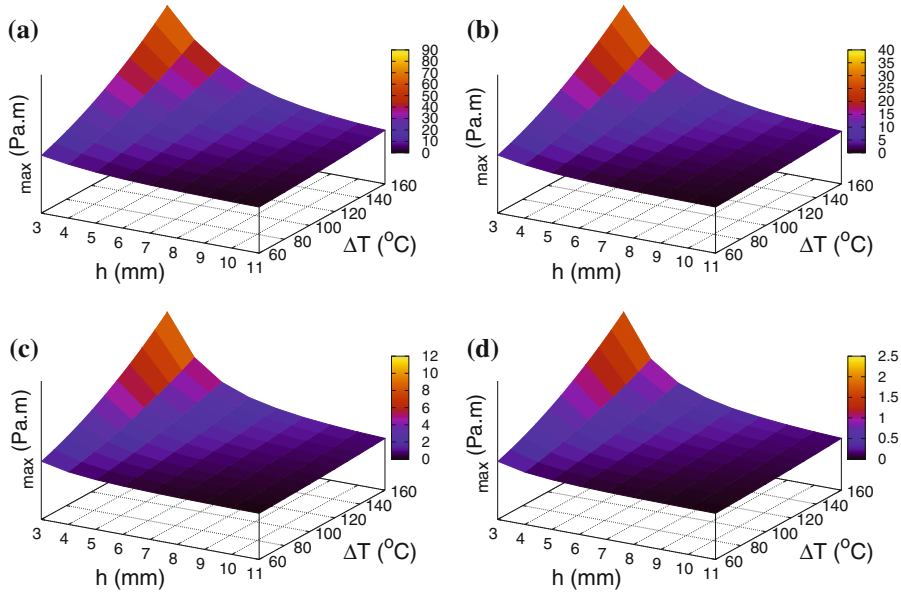

Fig. 6 Energy release rate as a function of the temperature ΔT and the distance water-oven h for different plate widths: **a** $w = 12$ mm, **b** $w = 10$ mm, **c** $w = 8$ mm and **d** $w = 6$ mm

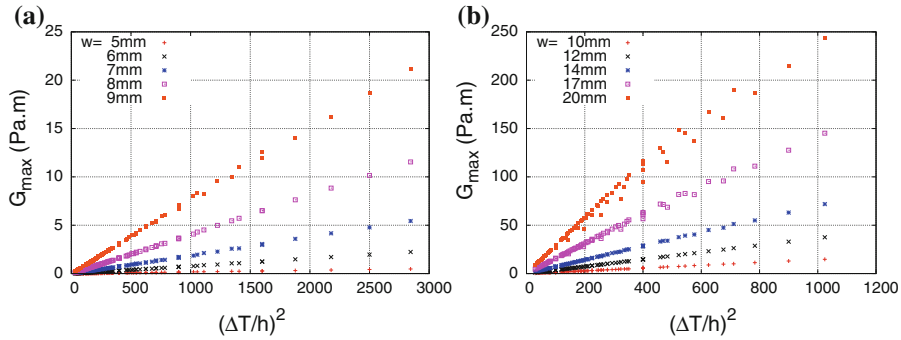

Fig. 7 Energy release rate as a function of the ratio $(\Delta T/h)^2$ for different plate widths w: **a** $w \in \{5,\ 6,\ 7,\ 8\ ,9$ mm$\}$ and **b** $w \in \{10,\ 12,\ 14,\ 17,\ 20$ mm$\}$

$\Delta T \in \{60, 70, 80, 90, 100, 110, 120, 130, 140, 150, 160°\text{C}\}$ gives a value for $G_{\max}$ reported in Fig. 6b. The whole Fig. 6b is summarized by a simple dot in Fig. 8a, i.e. $w = 10$ mm and $ratio = 0.0033$.

However, Fig. 8a shows that there is still a dependence with the plate width. The formulation is corrected with an additional factor depending on the plate width w only. One obtains an analytical formula denoted by G^{an}_{max} for the maximum of the energy release rate:

$$G^{an}_{\max} = 0.0025\ E \left(\alpha \Delta T \frac{w}{h}\right)^2 w \left(\frac{w}{w_0} - 1\right) \qquad (14)$$

where $w_0 = 4.5$ mm. A Least Square Estimation was involved in order to perform the numerical fitting of Eq. (12) with Fig. 8a, i.e. the determination of the parameters w_0 and 0.0025 in Eq. (14). Fig. 8b shows the ratio between the numerical G_{max} and the analytical $G^{an}_{\max}$ obtained after the analysis. The ratio oscillates between 90% and 118%, which gives an error of 18% maximum for a plate width of about 13 mm. Otherwise, the formula given in Eq. (14) is a good indicator to estimate the maximum of the energy release rate from the knowledge of the experiment.

4.5 Conclusion on the experiment parameters study

Figure 9a shows the maximum energy release rate as a function of the plate width for different distance water-oven h and temperature gap ΔT.

It shows that the increase of the plate width leads to a greater maximum energy release rate. This means that a greater plate width increases the probability of a crack propagation occuring. Experimentaly, Ronsin et al. (1995), Ronsin and Perrin (1998) observed such an effect of the plate width on the crack propagation;

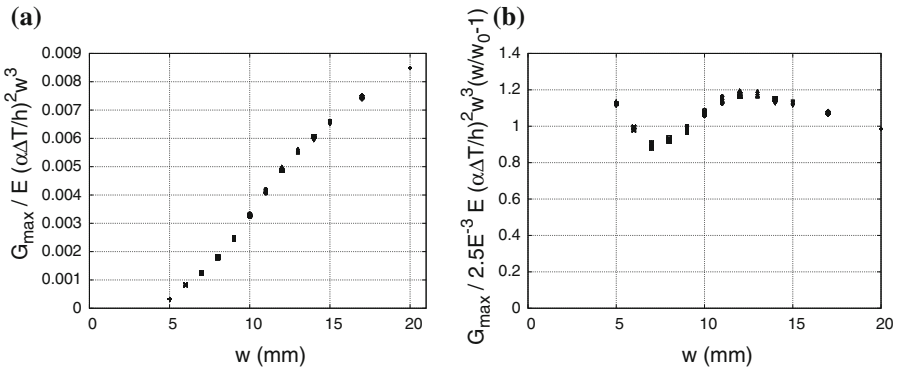

Fig. 8 Normalized maximum energy release rate as a function of the plate width: **a** normalization by $E\left(\alpha\Delta T\frac{w}{h}\right)^2 w$ and **b** by $0.0025E\left(\alpha\Delta T\frac{w}{h}\right)^2 w\left(\frac{w}{w_0}-1\right)$ with $w_0 = 4.5$ mm; for each width several $G_{\max}$ were computed with $\Delta T \in [60; 160°C]$ and $h \in [3; 11\,\text{mm}]$ as shown in Fig. 6

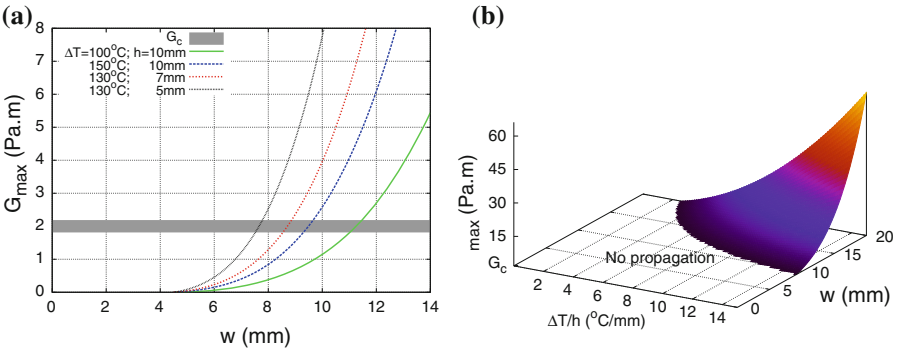

Fig. 9 Maximum of the energy release rate: **a** as a function of the plate width w for different distance water-oven h and temperature ΔT, and **b** as a function of the plate width w and temperature gradient $\Delta T/h$ for very small velocity V (only $G > G_c$ is represented)

they pointed out a critical plate width for the transition from non propagating to propagating crack. The following result can be extracted: for $h = 5$mm and $\Delta T = 130°C$, the energy release is above the critical value for a plate width of about 7.8 mm. Experimentally, Ronsin et al. (1995); Ronsin and Perrin (1998) found a plate width of 8 mm. This configuration corresponds to the transition from non propagating to propagating crack.

Figure 9b presents the analytical formula of the maximum of the energy release rate as a function of the plate width w and temperature gradient $\Delta T/h$ for very small velocity V. It shows the region $(\Delta T/h;\ w)$ where this maximum is greater than the critical energy release rate G_c, and thus whether or not the crack will propagate.

5 Numerical simulation of crack propagation

5.1 Straight crack propagation

We consider the following numerical experiments: a plate whose width is $w \in \{10; 14; 20\,\text{mm}\}$ is moved from an oven at different temperatures into a bath of water 10 mm below, at temperature 20°C. Figure 9a shows that the maximum of the energy release rate for these settings are above the critical value G_c. According to this statement, the crack is expected to propagate, because the loading condition and geometry make the maximum of the energy release rate greater than the critical value G_c.

We first observed that the crack propagates straight for the three simulations. Figure 10a presents the crack length as a function of time: it shows that the crack propagates at a constant velocity 0.1 mm/s which corresponds to the dipping velocity V. According to Eq. (11), the vertical crack position z in the global basis (X, Y) shown in Fig. 1 becomes constant. Indeed Fig. 10b presents the vertical position of the crack tip as a function of time; it can be seen that the crack tip moves down at velocity V when it is in the oven, then remains at the same vertical position during the remaining time of the simulation. Figure 10c, respectively 10(d), presents the mode 1 stress intensity factor, respectively the energy release rate, as a function of time. One can notice that the stress intensity factor and the energy release rate remain constant during the propagation of the crack, and their respective values are close to the critical one.

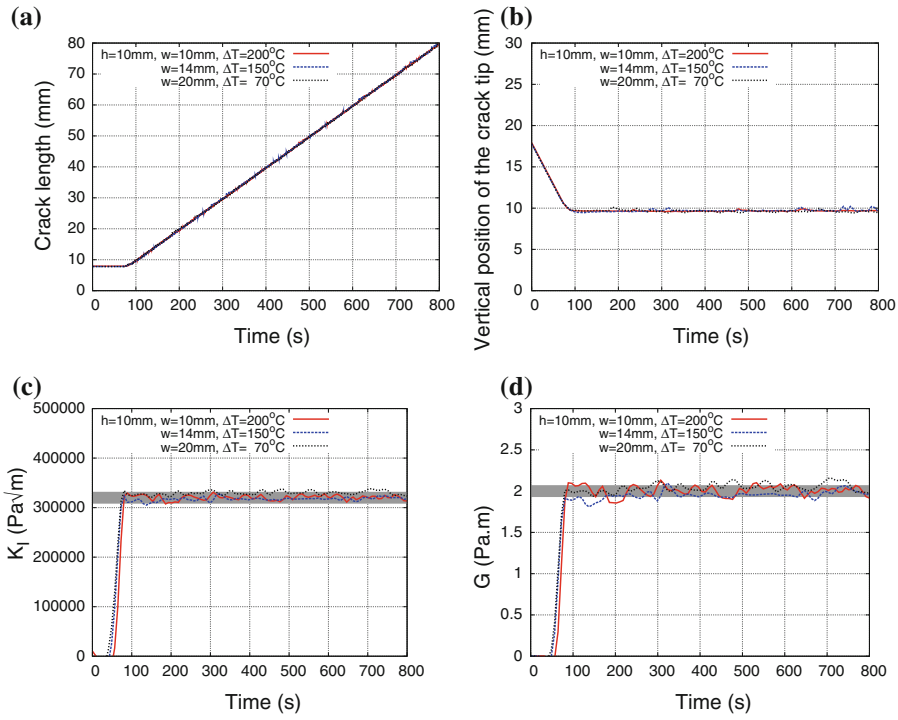

Fig. 10 **a** crack length, **b** vertical position of the crack tip, **c** mode 1 stress intensity factor and **d** energy release rate as a function of time for the straight crack propagation obtained with a dipping velocity of $V = 0.1$ mm/s

5.2 Oscillatory crack propagation

5.2.1 Catching the oscillatory behavior of the crack

In order to reach an oscillatory behavior of the crack, the loading, i.e. the temperature difference ΔT, is increased. The same regular mesh is still used.

The crack paths results are shown in Fig. 11 for three different plate widths: (a) $w = 10$ mm, (b) $w = 14$ mm and (c) $w = 20$ mm. It also presents crack trajectories for different loadings. The results show that above a certain loading, the straight crack propagation becomes oscillatory, and the oscillations are quite smooth. In Fig. 11b, respectively Fig. 11c, an increase of the temperature difference from 155 to 160°C, respectively 70 to 75°C, make the crack oscillate. Figure 11a shows a very smooth regular oscillatory crack path.

For the test run with $h = 10$ mm, $w = 10$ mm and $\Delta T = 200$°C, Fig. 12 presents the vertical crack tip position as a function of time. It can be seen that the crack tip remains at the entrance of the oven during the crack propagation. This is the same observation as for the straight crack path. Nevertheless the crack tip position oscillates in the X direction as shown in Fig. 11a. Figure 13 presents the energy release rate as a function of time. It shows that the energy release rate remains constant during the whole propagation; its value is close to the critical one G_c.

In order to compare with the experiment, Fig. 14 shows an experimental result obtained by Ronsin and Perrin (1998). According to Figs. 11c and 14, the shape of the numerical crack path shows the same curvature as the experimental one, also presented in Ronsin et al. (1995), Yang and Ravi-Chandar (2001). A good agreement between computation and experiment is shown in term of crack path. Unlike in Ferney et al. (1999), there is no dependence in the crack path due to the mesh in XFEM. Compared to the inter element method (Ferney et al. 1999) whose result clearly shows a mesh dependence, the results corresponding to the boundary element method (Yang and Ravi-Chandar 2001) and XFEM agree well with the experiment. However the mesh used with XFEM is about five times coarser then the ones used within the interelement method (Ferney et al. 1999) or the boundary element method (Yang and Ravi-Chandar 2001). Thus the XFEM formulation shows an important improvement compared to the interelement method, and a small improvement compared to the boundary element method, because it does not require adaptive mesh or remeshing.

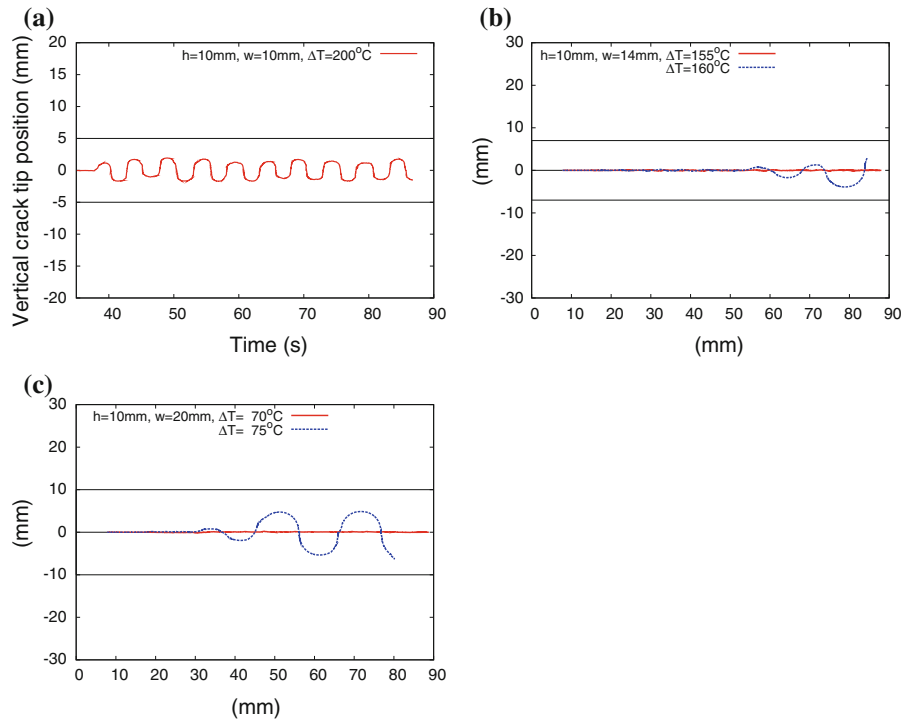

Fig. 11 Crack trajectories for different temperature differences ΔT and different plate widths: **a** plate width $w = 10$ mm, **b** plate width $w = 14$ mm and **c** $w = 20$ mm

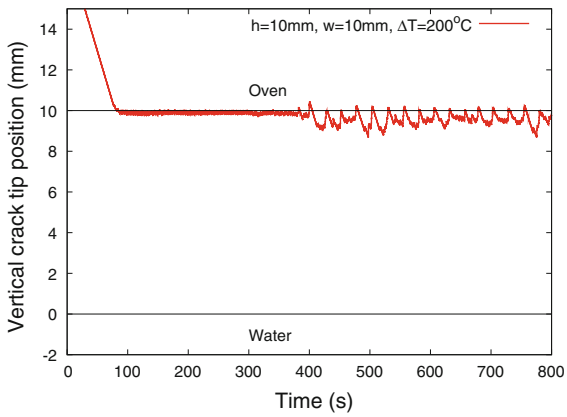

Fig. 12 Vertical crack tip position as a function of time for the test run with a plate width $w = 10$ mm (see Fig. 11(**a**) for corresponding crack path)

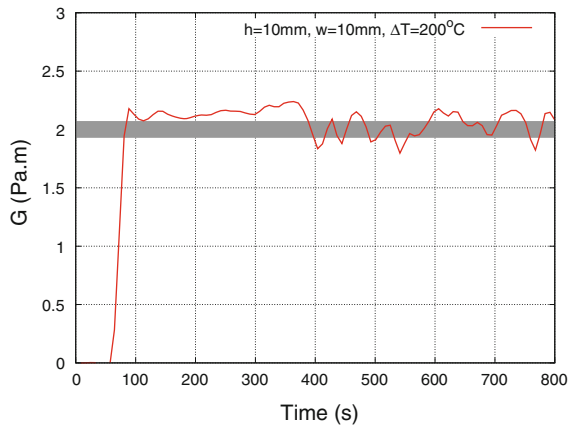

Fig. 13 Energy release rate as a function of time for the test run with a plate width $w = 10$ mm (see Fig. 11**a** for corresponding crack path)

5.2.2 Maximum hoop stress criterion versus Local Symmetry criterion

This section focuses on the study of the crack path with the criteria, i.e. maximum hoop stress criterion and Local Symmetry criterion (also called "$K_2 = 0$" criterion). This aims at evaluating the difference in term of the oscillatory crack path given by the two criteria, i.e. wavelength and amplitude.

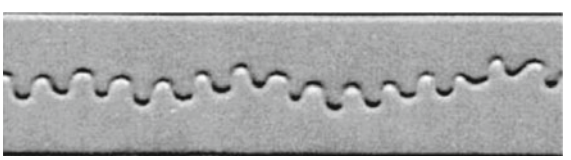

Fig. 14 Experimental oscillatory crack path obtained by Ronsin and Perrin (1998)

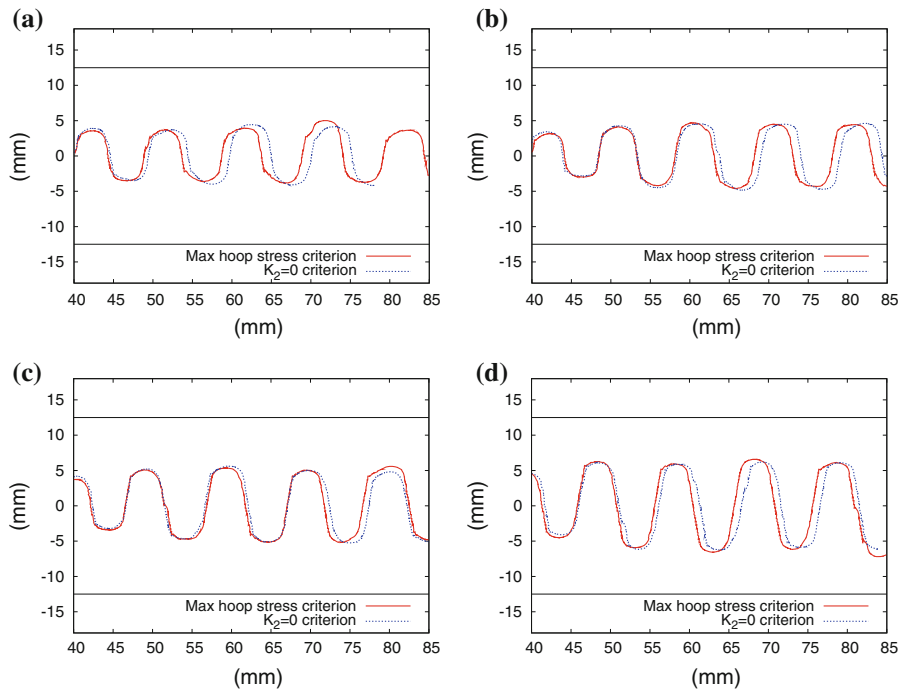

Fig. 15 Crack paths for different temperature differences simulated with both criteria: maximum hoop stress criterion and "$K_2 = 0$" criterion: **a** 52°C, **b** 62°C, **c** 82°C and **d** 104°C

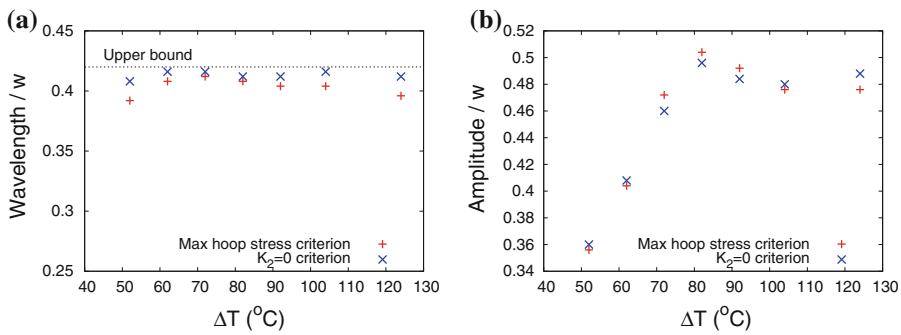

Fig. 16 **a** Wavelength and **b** amplitude of the oscillatory crack path as a function of the temperature difference simulated with both criteria, maximum hoop stress criterion and "$K_2 = 0$" criterion

Let us consider a plate whose width is 25 mm in order to compare the results with Yang and Ravi-Chandar (2001). The dimensions of the plate are 100 mm × 25 mm, and the corresponding mesh is 200 × 51 4-node elements. The space discretization method is still XFEM for modeling the crack within the mesh. Several simulations have been run with different temperature and the two different criteria.

Figure 15 shows the two crack paths obtained with both criteria, for different temperatures; (a) 52°C, (b) 62°C, (c) 82°C and (d) 104°C. The criteria give similar results in term of crack path and curvature. In addition, the amplitude of the oscillatory paths are very close. However, the Local Symmetry criterion tends to have a greater wavelength than the maximum hoop stress criterion.

Figure 16a presents the wavelength of each path shown in Fig. 15 as a function of the temperature difference. The two fracture criteria give similar results: less than 5% difference is shown on the wavelength given by the two criteria. However the Local Symmetry criterion ("$K_2 = 0$" criterion) tends to give a slightly greater wavelength than the maximum hoop stress criterion. This observation agrees with Eq. (10) given by the algorithm to determine both direction; this Equation showed that the Local Symmetry criterion is slightly smaller than the maximum hoop stress criterion. Therefore the corresponding oscillations wavelength is slightly

greater. Although both results in Fig. 15 show a good agreement with Yang and Ravi-Chandar (2001) emphasizing a upper bound limit for the wavelength independent of the temperature difference, the present limit is slightly below 0.42 whereas Yang and Ravi-Chandar (2001) observed 0.40.

Figure 16b presents the amplitude of the oscillation of the crack paths shown in Fig. 15 as a function of the temperature difference. Both criteria agree well with each other within 4%. The global behavior of the crack is that the oscillation amplitude increases with the temperature loading ΔT from 50 to 90°C. Then the oscillation amplitude becomes independent of the temperature. For higher temperature than 130°C, the experimental observations (Ronsin and Perrin 1998; Yang and Ravi-Chandar 2001) show that the crack path may not be oscillatory anymore, but turns into a unpredictible path, and where even branches occur (Ronsin and Perrin 1998; Yang and Ravi-Chandar 2001).

6 Conclusion

In this paper, an experiment where a crack propagation occurs in a glass plate under thermal loading was numerically investigated. The propagation showed a straight or oscillatory crack path.

First, we focused on the transition from non propagation to propagation by analyzing the influence of the experimental parameters on the maximum of the energy release available.

The analysis of the experiment dealing with a thermal crack propagation in a glass plate was next described. It showed more particularly the energy release rate given by the setting or configuration of the experiment, and thus allowed to conclude whether crack propagation is likely to occur. A general analytical formulation of the maximum of the energy release rate was proposed for a quite wide range of experimental settings such as the geometry of the plate and the temperature gradient. This became a good indicator to estimate or predict crack propagation based on the experimental settings only.

Second, we computed crack propagations for different loadings and plate widths: straight and oscillatory crack paths were obtained. Indeed, the observed straight and oscillatory crack paths were recovered by the computation. The numerical oscillatory crack path also showed a good agreement with the experimental observation in terms of curvature. The numerical tool used here (i.e. XFEM) efficiently provided reasonable results for such experiment, and avoided mesh dependence in the results.

Third, we analyzed the results given in term of crack path for the two different criteria: the maximum hoop stress criterion and the Local Symmetry criterion. Both results were similar, but a closer look on the wavelength and amplitude of the oscillatory paths showed slight differences between the criteria. This studied experiment brought some results in term of comparison of the fracture criteria by analyzing the oscillatory crack paths. Although both criteria agreed well with each other, a small difference in the wavelength of the paths could be shown in such experiment.

Acknowledgments The support of the Office of Naval Research under Grants N00014-08-1-1191 and N00014-09-1-0030 and also the Army Research Office under Grant W911NF-008-1-0212 is gratefully acknowledged.

References

Adda-Bedia M, Arias R, Ben Amar M, Lund F (1999) Generalized Griffith criterion for dynamic fracture and the stability of crack motion at high velocities. Phys Rev E 60(2):2366–2376

Adda-Bedia M, Pomeau Y (1995) Crack instabilities of a heated glass strip. Phys Rev E 52:4105

Amestoy M, Leblond JB (1992) Crack paths in plane situations–II. Detailed form of the expansion of the stress intensity factors. Int J Solids Struct 29(4):465–501

Attigui M, Petit C (1997) Mixed-mode separation in dynamic fracture mechanics : New path independent integrals. Int J Fract 84(1):19–36

Bahr HA, Fischer G, Weiss HJ (1986) Thermal-shock crack patterns explained by single and multiple crack propagation. J Mater Sci 21(8):2716–2720

Bahr HA, Gerbatsch A, Bahr U, Weiss HJ (1995) Oscillatory instability in thermal cracking: a first-order phase-transition phenomenon. Phys Rev E 52(1):240–243

Belytschko T, Black T (1999) Elastic crack growth in finite elements with minimal remeshing. Int J Numer Methods Eng 45(5):601–620

Belytschko T, Liu WK, Moran B (2000) Nonlinear finite elements for continua and structures. Wiley, Chichester

Belytschko T, Moës N, Usui S, Parimi C (2001) Arbitrary discontinuities in finite elements. Int J Numer Methods Eng 50(4):993–1013

Buckingham E (1915) The principle of similitude. Nature 96 (3):396–397

Corson F, Adda-Bedia M, Henry H, Katzav E (2009) Thermal fracture as a framework for quasi-static crack propagation. Int J Fract 158:1–14

Cotterell B, Rice JR (1980) Slightly curved or kinked cracks. Int J Fract 16(2):155–169

Deegan RD, Chheda S, Patel L, Marder M, Swinney HL, Kim J, de Lozanne A (2003) Wavy and rough cracks in silicon. Phys Rev E 67(6):66209

Erdogan F, Sih GC (1963) On the crack extension in plates under plane loading and transverse shear. J Basic Eng 85:519–527

Ferney BD, De Vary MR, Hsia KJ, Needleman A (1999) Oscillatory crack growth in glass. Scripta materialia 41(3):275–281

Freund LB (1972) Crack Propagation in an elastic solid subjected to general loading. Pt. 1. Constant rate of extension. J Mech Phys Solids 20(3):129–140

Gol'dstein RV, Salganik RL (1974) Brittle fracture of solids with arbitrary cracks. Int J Fract 10(4):507–523

Griffith AA (1921) The phenomena of rupture and flow in solids. Philosophical transactions of the royal society of london. Series A, containing papers of a mathematical or physical character, pp 163–198

Hakim V, Karma A (2009) Laws of crack motion and phase-field models of fracture. J Mech Phys Solids 57(2):342–368

Katzav E, Adda-Bedia M, Arias R (2007) Theory of dynamic crack branching in brittle materials. Int J Fract 143(3):245–271

Katzav E, Adda-Bedia M, Derrida B (2007) Fracture surfaces of heterogeneous materials: a 2D solvable model. EPL (Europhys Lett) 78:46006

Kilic B, Madenci E (2009) Prediction of crack paths in a quenched glass plate by using peridynamic theory. Int J Fract 156(2):165–177

Marder M (1994) Instability of a crack in a heated strip. Phys Rev E 49(1):51–54

Menouillard T, Elguedj T, Combescure A (2006) Mixed mode stress intensity factors for graded materials. Int J Solids Struct 43:1946–1959

Menouillard T, Réthoré J, Combescure A, Bung H (2006) Efficient explicit time stepping for the eXtended Finite Element Method (X-FEM). Int J Numer Methods Eng 68:911–939

Menouillard T, Réthoré J, Moës N, Combescure A, Bung H (2008) Mass lumping strategies for X-FEM explicit dynamics: application to crack propagation. Int J Numer Methods Eng 74(3):447–474

Moës N, Dolbow J, Belytschko T (1999) A finite element method for crack growth without remeshing. Int J Numer Methods Eng 46(1):131–150

Needleman A (1987) A continuum model for void nucleation by inclusion debonding. J Appl Mech 54:525

Pham VB, Bahr HA, Bahr U, Balke H, Weiss HJ (2008) Global bifurcation criterion for oscillatory crack path instability. Phys Rev E 77(6):66114

Pla O (1996) Modelling fracture driven by a thermal gradient. Model Simul Mater Sci Eng 4(2):193–202

Reddy KPR, Fontana EH, Helfinstine JD (1988) Fracture toughness measurement of glass and ceramic materials using chevron-notched specimens. J Am Ceram Soc 71(6):310–313

Rice JR (1968) A path independent integral and the approximate analysis of strain concentration by cracks and notches. J Appl Mech (Trans ASME) 35:379–386

Ronsin O, Heslot F, Perrin B (1995) Experimental study of quasistatic brittle crack propagation. Phys Rev Lett 75(12):2352–2355

Ronsin O, Perrin B (1997) Multi-fracture propagation in a directional crack growth experiment. Europhys Lett 38(6):435–440

Ronsin O, Perrin B (1998) Dynamics of quasistatic directional crack growth. Phys Rev E 58(6):7878–7886

Sasa S, Sekimoto K, Nakanishi H (1994) Oscillatory instability of crack propagations in quasistatic fracture. Phys Rev E 50(3):1733–1736

Yang B, Ravi-Chandar K (2001) Crack path instabilities in a quenched glass plate. J Mech Phys Solids 49(1):91–130

Yoneyama S, Sakaue K, Kikuta H, Takashi M (2008) Observation of stress field around an oscillating crack tip in a quenched thin glass plate. Exp Mech 48(3):367–374

Yuse A, Sano M (1993) Transition between crack patterns in quenched glass plates. Nature 362:329–331